

HST Fine Guidance Sensor Parallaxes for Four Classical Novae^{1,2}

Thomas E. Harrison³, Jillian Bornak

Department of Astronomy, New Mexico State University, Box 30001, MSC 4500, Las
Cruces, NM 88003-8001

tharriso@nmsu.edu, jbornak@nmsu.edu

Barbara E. McArthur and G. Fritz Benedict

McDonald Observatory, University of Texas, Austin, TX 78712

mca@barney.as.utexas.edu, fritz@astro.as.utexas.edu

Received _____; accepted _____

ABSTRACT

We have used data obtained with the Fine Guidance Sensors on the *Hubble Space Telescope* to derive precise astrometric parallaxes for four classical novae: V603 Aql, DQ Her, GK Per, and RR Pic. All four objects exceeded the Eddington limit at visual maximum. Re-examination of the original light curve data for V603 Aql and GK Per has led us to conclude that their visual maxima were slightly brighter than commonly assumed. With known distances, we examine the various maximum magnitude–rate of decline (MMRD) relationships that have been established for classical novae. We find that these four objects show a similar level of scatter about these relationships as seen in larger samples of novae whose distances were determined using indirect techniques. We also examine the nebular expansion parallax method, and find that it fails for three of the four objects. In each case it was possible to find an explanation for the failure of that technique to give precise distance estimates. DQ Her appears to suffer from an anomalously high extinction when compared to field stars on its sight line. We suggest that this is likely due to local material, which may also be the source of the *IRAS* detections of this object.

Key words: parallaxes — stars: novae, cataclysmic variables — stars: individual (V603 Aquilae, DQ Herculis, GK Persei, RR Pictoris)

¹Based partially on observations made with the NASA/ESA Hubble Space Telescope, obtained from the Data Archive at the Space Telescope Science Institute, which is operated by the Association of Universities for Research in Astronomy, Inc., under NASA contract NAS 5-26555. These observations are associated with programs GO10912, GO11295, and GO11785.

²Based partially on observations obtained with the Apache Point Observatory 3.5-meter telescope, which is owned and operated by the Astrophysical Research Consortium.

³Visiting Astronomer, Cerro Tololo Inter-American Observatory, National Optical Astronomy Observatory, which is operated by the Association of Universities for Research in Astronomy, Inc., under cooperative agreement with the National Science Foundation.

1. Introduction

Classical novae (CNe) are thermonuclear explosions on the surface of a white dwarf that has been accreting material for thousands of years from its low mass companion. Townsley & Bildsten (2004) show that for cataclysmic variable systems with mass accretion rates of $\dot{M} = 10^{-8}$ to $10^{-10} M_{\odot}$ yr $^{-1}$, CNe ignition can occur once the accumulated envelope on the white dwarf reaches 10^{-4} to $10^{-5} M_{\odot}$. The resulting eruption can reach well beyond the Eddington limit, and eject $\approx 10^{-4} M_{\odot}$ of enriched material at high velocity. With the most luminous eruptions reaching to $M_V \leq -9.0$, and due to the fact that they occur in all types of galaxies, CNe have been proposed as useful extragalactic distance indicators (van den Bergh & Pritchett 1986; Della Valle & Livio 1995; Della Valle & Gilmozzi 2002). In addition, however, the eruptions of CNe provide critical tests of our understanding of thermonuclear runaways, the nucleosynthesis that occurs within the burning layers (c.f., Starrfield et al. 2009), and the factors that drive and shape the shell ejection process.

To fully understand the outbursts of CNe, it is essential to have precise distances. While a wide range of secondary distance estimation techniques have been applied to CNe, none have had high precision parallaxes measured. The most reliable indirect method for estimating CNe distances has come from “nebular expansion parallaxes”. This technique combines spectroscopically determined expansion velocities, and the observed nebular remnant shell size, to estimate the distance. For the earliest attempts to employ this technique, the velocity of the “principal absorption component” (see Payne-Gaposchkin 1957, or Warner 2008) was used to estimate the expansion velocity of the bulk of the ejecta. Unfortunately, such spectra are only seen near visual maximum, and thus rarely observed for most CNe. More recent efforts (see the review by O’Brien & Bode 2008) employ a kinematic model derived from spectroscopic observations of the resolved shell. This regimen is much more robust, in that it allows compensation for the tendency of CNe to have

prolate, ellipsoidal remnants (Wade et al. 2000).

One of the long-standing correlations in the field of CNe, dating back to McLaughlin (1945), is that the *speed* of the outburst is related to the peak luminosity of the eruption. McLaughlin used a variety of distance estimation techniques to derive the absolute visual magnitudes at maximum, and correlated this with the time it took for the CNe to dim by three magnitudes from visual maximum (“ t_3 ”). There have been a number of attempts to calibrate a maximum magnitude–rate of decline (MMRD) relationship for CNe. Downes & Duerbeck (2000) have produced the most recent updates (though see Hachisu & Kato 2010), including the two linear laws (involving t_2 and t_3), as well as the arctangent law (that uses t_2) first formulated by Della Valle & Livio (1995). The conclusion of Downes & Duerbeck was that a scatter of 0.5 mag was present in all of these relationships, and indicated that a second parameter (beyond white dwarf mass) could be influencing the outburst luminosities of CNe.

Given the number of uncertainties that go into the derivation of the distances using the secondary techniques, the reliability of these methods/relationships has yet to be proven. What is needed to examine these techniques is high precision parallaxes. Using data obtained with the Fine Guidance Sensors on the *HST*, we have derived precise parallaxes for four CNe: V603 Aql, DQ Her, GK Per, and RR Pic. We use the distances for this small sample to explore the nebular expansion parallax methods as applied to these sources, as well as to test the various MMRD relations. In the next section we describe the observations required to obtain parallaxes with the Fine Guidance Sensors, in section 3 we provide a brief overview of how parallaxes are obtained from such data, in section 4 we discuss the results for the individual CNe, and in section 5 we state our conclusions.

2. Observations

The Fine Guidance Sensors (FGS), besides providing guiding for the other science instruments on *HST*, can be used to obtain precision astrometry. Details on the FGS instrument can be found in Nelan et al. (2011). The main benefits of the FGSs are their large fields-of-view ($3' \times 10'$), and high dynamic range. Benedict et al. (2011) have thoroughly described how an astrometric program is conducted with the FGS, and we refer the reader to that discussion. Here we provide a brief overview of the process.

2.1. *HST* FGS Data

A single “POS Mode” FGS observation consists of multiple measurements of the relative positions of the astrometric target and a set of reference frame stars. During this single *HST* orbit, a typical astrometric sequence will result in the target being observed four or five times relative to the reference frame stars. The entire field is then observed at several well-separated epochs. For a sufficiently bright target ($V \leq 15.0$) and a well-populated reference frame, ten orbits of FGS observations can produce parallaxes that have precisions of $\sigma_\pi \leq \pm 0.25$ mas. For this particular program, with data from three *HST* cycles (GO10912, GO11295, and GO11785), between eight and ten sets of astrometric data were acquired with *HST* FGS 1r for each CNe. Most of these data were obtained at epochs close to the time of maximum parallax factor (though occasionally tempered by two-gyro guiding constraints, see Benedict et al. 2010). Thus, only small segments of the parallactic ellipses were observed for these targets. The various complete data aggregates span from 2.42 to 3.28 years.

Approximately forty minutes of spacecraft time were used to obtain each individual *HST* data set. These data were then reduced and calibrated as detailed in McArthur

et al. (2001), and Benedict et al. (2002a, 2002b). At each epoch the positions of the reference stars and the target were measured several times to correct for intra-orbit drift (see Fig. 1 of Benedict et al. 2002a). Data were downloaded from the *HST* archive and pipeline-processed. The FGS data reduction pipeline extracts the measurements (the x and y positions from the fringe tracking, acquired at a 40 Hz rate, yielding hundreds of individual measurements), extracts the median, corrects for the Optical Field Angle Distortion (c.f. McArthur et al. 2002), and adds the required time tags and parallax factors.

2.2. Ground-based Photometry and Spectroscopy

As described below, to solve for the parallax of a program object using the FGS, we need to estimate the parallaxes of the reference frame stars. We use spectra to classify the temperature and luminosity class of each star, and then combine these with $UBVRIJHK$ photometry to determine their visual extinctions.

We obtained spectra of the reference frame stars for the three northern CNe using the Dual Imaging Spectrograph⁴ (“DIS”) on the 3.5 m telescope at the Apache Point Observatory. DIS simultaneously obtains spectra covering blue and red spectral regions, and with the high resolution gratings (1,200 line/mm) provides dispersions of 0.62 Å/pix in the blue, and 0.58 Å/pix in the red. For RR Pic, we obtained spectra of the reference frame stars using the R–C Spectrograph⁵ on the Blanco 4 m telescope at Cerro Tololo Interamerican Observatory (program 2009A-0009). The KPGL1 grating was used, and with the “Loral 3K” detector, provided a dispersion of 1.01 Å/pix.

Optical photometry for the fields of V603 Aql, DQ Her, and GK Per were obtained

⁴<http://www.apo.nmsu.edu/arc35m/Instruments/DIS/>

⁵http://www.ctio.noao.edu/spectrographs/4m_R-C/4m_R-C.html

using the robotic New Mexico State University (NMSU) 1 m telescope (Holtzman et al. 2010) at Apache Point Observatory. The NMSU 1 m is equipped with an E2V 2048 sq. CCD camera, and the standard Bessell *UBVRI* filter set. Photometry of the field of RR Pic was obtained using the Tek2K CCD imager⁶ on the SMARTS 0.9 m telescope at CTIO (program 2009A-0009). The images for the four CNe fields, along with the appropriate calibration data, were obtained in the usual fashion, reduced using IRAF, and flux calibrated with observations of Landolt standards.

Over the past decade, we have compiled an extensive set of template spectra covering a large range of temperature and luminosity classes in support of our various FGS programs on both the APO 3.5 m, and the Blanco 4 m. We perform MK classification of each of the reference frame stars with respect to these templates, as well as use the temperature and luminosity classification characteristics listed in Yamashita et al. (1978). We find that for well exposed DIS spectra, our temperature classifications are generally good to ± 1 subclass. For the lower resolution CTIO data, however, there is more uncertainty, and we generally obtain spectral classifications with uncertainties of ± 2 subclasses.

Note that we are bound to encounter both subgiants and unresolved binaries in a program with this many reference stars. For example, in Table 1 we identify DQ Her Ref #01 as a potential binary because the parallax derived from our astrometric solution was much smaller than its spectroscopic parallax. We identify possible binaries and subgiants from their large residuals in the astrometric solution. First, the astrometric reference frame is modeled without the target CNe, as a check on the input spectroscopic parallaxes and proper motions. When the model fit to the reference frame is poor, we examine the reference stars individually, first by removal looking for a significant χ^2 improvement, and secondly by treating those outliers as targets to redetermine a more likely a priori input

⁶<http://www.ctio.noao.edu/noao/content/tek2k>

parallax. We then confirm that this re-classification is consistent with the spectroscopic and photometric data. These redetermined spectroscopic parallax values are then used as input in the final astrometric model that includes the target CNe.

With the spectral classification of the reference stars complete, we then use the *UBVRI* photometry we have obtained, in conjunction with *JHK* photometry from 2MASS, to derive the visual extinction to the sources using the reddening relationships from Rieke & Lebofsky (1985). Once determined, we can estimate spectroscopic parallaxes using the absolute visual magnitude calibrations for main sequence stars listed in Houk et al. (1997), and for giant stars using Cox (2000). We assemble all of the relevant data for the reference frame stars in Table 1. The first column of this table lists the object identification, the second and third list the position (J2000), and the fourth and fifth columns list the proper motions (in mas yr⁻¹) as determined from our astrometric solution. The sixth column lists the derived spectral type of the reference frame star, the seventh column is its *V* magnitude, the eighth is its (*B* − *V*) color, the penultimate column lists the visual extinction estimate, and the final column lists the parallax (with error) computed from the astrometric solution (but advised by the input spectroscopic parallax).

In Fig. 1, we plot the derived visual extinctions vs. the distances to the reference frame stars listed in Table 1. In each figure we indicate the average line-of-sight value for the extinction in the direction of the program CNe using the IRSA Galactic Dust Reddening and Extinction calculator⁸ (except for V603 Aql, where the line-of-sight extinction is enormous: $A_V > 15$ mag). In this figure we also denote the location of the program CNe with crosses (discussed below).

⁸<http://irsa.ipac.caltech.edu/applications/DUST/>

3. Deriving Parallaxes for the Program CNe

With the x and y positions from the FGS 1r observations in hand, we proceed to determine the scale, rotation, and offset “plate constants” for each epoch relative to a constraint epoch (the “master plate”). We employ GaussFit (Jefferys et al. 1988) to simultaneously minimize the χ^2 value for the following set of equations:

$$x' = x + lc_x(B - V) \quad (1)$$

$$y' = y + lc_y(B - V) \quad (2)$$

$$\xi = Ax' + By' + C - \mu_x \Delta t - P_\alpha \pi_x \quad (3)$$

$$\eta = Dx' + Ey' + F - \mu_y \Delta t - P_\delta \pi_y \quad (4)$$

In the first two equations, x and y are the measured coordinates from the FGS, and lc_x and lc_y are the lateral color correction terms that are dependent on the $(B - V)$ color of each star. A , B , D , and E are scale and rotation plate constants, C and F are offsets, μ_x and μ_y are the proper motions, Δt is the epoch difference from the mean epoch, P_α and P_δ are the parallax factors, while π_x and π_y are the parallaxes in x and y . The parallax factors are obtained from a JPL Earth orbit predictor (Standish 1990), version DE405. This set of equations was used for deriving the parallaxes of V603 Aql and RR Pic. For DQ Her, a four parameter solution was used (versus the six parameter solution shown above), having identical scale factors for x and y : $D \equiv -B$ and $E \equiv A$. For GK Per, we used a similar scheme as that for DQ Her (identical scale coefficients in x and y), but included additional radial scale terms into equations 3 and 4:

$$\xi = Ax' + By' + C + R_x(x^2 + y^2) - \mu_x \Delta t - P_\alpha \pi_x \quad (5)$$

$$\eta = -Bx' + Ay' + F + R_y(x^2 + y^2) - \mu_y \Delta t - P_\delta \pi_y \quad (6)$$

3.1. Input Modeling Constraints and Reference Frame Residuals

In our astrometric analysis, the reference star spectroscopic parallaxes and their proper motions from the PPMXL proper catalog (Roeser et al. 2010) are not considered absolute, and were input as observations with associated errors. Typical errors on the proper motions are of order 5 mas yr⁻¹ in each coordinate. In addition, the lateral color and cross-filter calibrations, as well as the measured ($B - V$) color indices, were also considered as observations with error. Note that while the CNe exhibited orbitally modulated brightness changes, their ($B - V$) colors remain relatively constant over an orbit (see Bruch & Engle 1994). Therefore we did not include in the modeling a time-dependent color correction value for any of the CNe.

The calibration by McArthur et al. (2002) of the Optical Field Angle Distortion (OFAD) reduces the large distortions, of amplitude $\sim 1''$, seen across the field of the FGS 1r, to below 2 mas. The OFAD used for the present reduction and analysis of the FGS 1r data for the CNe has been updated with the post May 2009 servicing mission observations (McArthur et al. 2012, in preparation). To determine if there might be systematic effects at the 1 mas level that could be correctable, we investigated the reference frame x and y residuals against: 1) the position within the field-of-view, 2) the radial distance from the center of the field-of-view, 3) the V magnitude and/or ($B - V$) color of the reference star, and 4) the epoch of observation. No such trends were detected. The final parallax and proper motion values (with errors) obtained from our modeling of the FGS data for the program reference stars are listed in Table 1⁹

⁹A careful examination of Table 1 will show that the number of reference stars used for the

The casual reader might be surprised at the small size of the errors on the parallaxes of the reference stars listed in Table 1. These small errors are informed by the input spectrophotometric parallaxes and their inherent error in a quasi-Bayesian manner. Because of the intrinsic width of the main sequence, and the spectroscopic classification uncertainty, the reference star spectroscopic parallaxes typically have intrinsic input errors of order $\sim 25\%$. Distant reference stars can have input spectroscopic parallaxes of order $\pi \approx 0.25$ mas, and thus the error bar on such parallaxes can be of order a few tens of μ as. All errors in the reference star *a priori* data (proper motion and spectroscopic parallax inputs) are used, in a Bayesian fashion, by the GaussFit program to arrive at the final parameters for the reference frame. With eight to ten observational epochs, five or more reference frame stars per field, more than two of years of proper motion information, the final astrometric solution derives the reference frame parallaxes and errors. *The multiple measurements included into the astrometric analysis results in error bars on the parallaxes and proper motions that are smaller than their input values.* Note that the final reference star parallax errors are of order 8%, as are the errors on our program objects (see below). The errors on the parallaxes and proper motions of the reference stars listed in Table 1 are uncorrelated. These errors are

astrometric solution for GK Per was smaller than for the other CNe. Three of the program reference stars for this field (Ref #3, #6, and #10) showed large residuals that could not be reduced by multiple alternative models (e.g., models with different scale parameters, or models that omitted *a priori* values of parallax and proper motion for that reference star). One possible source of such residuals is a field star located close to the target ($\leq 5''$, see Nelan et al. 2011). Another is that the object could be a binary star with a significant reflex motion with an orbital period that is on order of the frequency of the observational epochs. Ref #5 was dropped due to it being very faint ($V = 15.8$) and red [$(B - V) = 1.1$]. The good news is that the remaining targets produced a very quiet reference frame.

influenced by the quasi-Bayesian inputs, and thus are not truly independent measurements (in contrast to those of our program objects). The precision of the parallax for a program object is a direct consequence of the quality of the astrometric solution for its reference frame. As demonstrated by Benedict et al. (2002b, their section 5.1), the error bars on the program object parallaxes derived using this methodology are conservative.

3.2. The Parallaxes of V603 Aql, DQ Her, GK Per, and RR Pic

For each of the CNe, we constrain $\pi_x = \pi_y$ in Equations 3 and 4 to obtain the final parallaxes and proper motions listed in Table 2. The precisions of the parallaxes in Table 2 are an indication of our internal, random error, and for the program CNe, these errors are $\approx \pm 0.2$ mas. To assess our external error, we have compared the parallaxes from previous FGS programs (Benedict et al. 2002b, Soderblom et al. 2005, McArthur et al. 2011) with results from *Hipparcos* (Perryman et al. 1997). Other than for the Pleiades (Soderblom et al. 2005), there are no significant differences between the results obtained with the FGS, and with those from *Hipparcos* for any object with high precision parallaxes.

Of the four program objects, the only one with a statistically significant *Hipparcos* parallax is V603 Aql. Due to its faintness ($V = 11.7$, Bruch & Engel 1994), V603 Aql was a difficult target for *Hipparcos*. The original *Hipparcos* catalog lists $\pi_{abs} = 4.21 \pm 2.59$ mas. The van Leeuwen (2007) re-reduction of the *Hipparcos* data yielded $\pi_{abs} = 4.96 \pm 2.45$ mas for V603 Aql. Both determinations agree with our measurement ($\pi_{abs} = 4.011 \pm 0.137$ mas), given their significant error bars.

3.3. The Lutz-Kelker-Hanson Correction to M_V

As noted long ago by Trumpler & Weaver (1953), a systematic error is introduced into the calibration of the luminosities for a group of objects when using parallax. Due to the fact that in nearly every stellar population, the number of stars in a sample increases with distance, stars with overestimated parallaxes will outnumber those with underestimated parallaxes. Lutz & Kelker (1973) showed that the size of the bias depends only on the ratio of σ_π/π . Here we have used the general formulation of Hanson (1979) to determine the corrections for the program CNe. We calculate the Lutz-Kelker-Hanson (“LKH”) bias for our CNe presuming that they all belong to the same class of object (old disk stars), and report the LKH correction to be applied to the object’s absolute visual magnitude in the final column of Table 2. Given the uncertainties in the peak visual magnitudes of the program CNe, these small adjustments are unimportant in characterizing the outbursts of the program CNe, and will be ignored in what follows.

4. Results

With the astrometric results, we investigate the outbursts of the program CNe with respect to their light curve decline rates. Below we assemble both the published t_2 and t_3 decline rates for the program novae, as well as review their light curves to examine the long-established values for their maximum visual magnitudes. The MMRD relationships critically depend on having precise values for both of these quantities, thus we feel it is important to review the origins of the previously published values for those data. Having precisely known distances also allows for the investigation of the expansion of the nebulae produced in each of the outbursts. Downes & Duerbeck (2000) provide a summary of the outbursts of each of these CNe, including distance estimates derived using nebular expansion parallaxes. We compare the new astrometric distances with the distances from

the nebular expansion parallaxes in Table 3. Except for GK Per, the astrometric distances for the CNe turn out to be smaller than those estimated by Downes & Duerbeck. We order our discussion alphabetically by constellation name.

4.1. V603 Aquilae

V603 Aql erupted in 1918 June, and due to its brightness, a comprehensive light curve was compiled (Campbell 1919). There were also numerous spectroscopic observations of the outburst, and those data have been discussed by Wyse (1940). The light curve presented by Campbell shows that the nova reached $m_v = -1.1$ on 9 June 1918. In Fig. 2, we present the light curve of V603 Aql close to this date from the data in Table III of Campbell. Note that there are nine visual magnitude estimates that have the nova as being brighter than $m_v = -1.1$. Six of these are due to E. E. Barnard (Yerkes). Note that we have used the “Corrected Magnitudes”, for which Campbell accounted for the “bias” of the observer. In fact, Barnard reported that the nova peaked at $m_v = -1.5$ on JD24211754.94, to which Campbell subsequently applied a correction of +0.1 mag. One might discount Barnard’s observations given the difficulty of estimating the magnitude of something that was so much brighter than any naked eye stars of that season, but on JD24211754.78, W. H. Pickering (Harvard College Observatory, Mandeville, Jamaica) estimated $m_v = -1.2$; fifteen minutes later (JD24211754.79) Barnard derived the same brightness.

The consistency of the data, and the reputation of the observers in question, suggests that V603 Aql easily exceeded the commonly quoted value of $m_v = -1.1$ at visual maximum. These data support a value of *at least* $m_v = -1.4$ for its maximum. The discrepant data point near those of peak brightness, $m_v = -0.7$ (at JD24211754.98), is due to Conroy (1918), an amateur astronomer based in Los Angeles. Conroy indicates that at the time of his estimate, V603 Aql was “much bluer than Vega”, suggesting that it had not yet

reached visual maximum. It is interesting to note in his spectroscopic survey of “old novae” Humason (1938) lists $m_v = -1.4$ for the maximum of V603 Aql. We tabulate the outburst characteristics of V603 Aql, and the other program novae, in Table 4.

As discussed above, it has long been suggested that there is a relationship for CNe between their absolute visual magnitudes at maximum, and the rate of decline in their light curves from visual maximum. We have averaged the reported t_2 and t_3 values from the literature (Duerbeck 1987; McLaughlin 1939; and Strope et al. 2010) for V603 Aql to arrive at the values listed in Table 4. The published values of these two quantities are all quite similar, due to the rather smooth decline of the light curve from maximum. Note that if we assume V603 Aql actually reached $m_v = -1.4$ at peak, the resultant t_2 and t_3 values are reduced to 1.5 d, and 6 d, respectively. The extinction to V603 Aql is low, with $E(B - V) = 0.07$ (Gallagher & Holm 1974). Using this, the new parallax, and $m_{v_{\max}} = -1.4$, we derive an absolute visual magnitude at maximum of $M_{V_{\max}} = -8.60$. Given the estimate for the mass of its white dwarf, $M_1 = 1.2 \pm 0.2$ (Arenas et al. 2000), at its peak, V603 Aql exceeded the Eddington limit by ~ 1.7 mag, but its super-Eddington phase (at visual wavelengths) only lasted ≈ 48 hr.

Besides an extensive discussion of the spectra of V603 Aql, Wyse (1940) compiled measurements of the size of the expanding nebular shell from the eruption of V603 Aql first noticed by Barnard (1919). With a precise parallax, we can determine the expansion velocity required to reproduce the observations. We plot the angular measurements of the disk of V603 Aql versus the time since outburst in Fig. 3. It is apparent from this figure that the expansion velocity needed to produce an ejected shell that evolved in the observed way was $\approx 1,100$ km s $^{-1}$. This value is much lower than the published velocities of the “principal absorption” components of 1,500 km s $^{-1}$ (McLaughlin 1940) or 1,700 km s $^{-1}$ (Payne-Gaposchkin 1957). Since it has long been believed that the principal absorption

component is the velocity of the bulk of the ejecta (e.g., Payne-Gaposchkin), it is somewhat surprising that the observed expansion of the nebula indicates a much lower velocity.

A possible way to reconcile these observations comes from a model of the ejected shell of V603 Aql constructed by Weaver (1974). Weaver finds that the spectroscopic record is consistent with a shell that has its long axis pointed towards the Sun. A recent estimate of the orbital inclination of the underlying binary arrives at $i = 13^\circ$ (Arenas et al. 2000). Thus, we view V603 Aql nearly pole-on. If we ratio the values of the observed “equatorial” expansion velocity with the principal absorption velocities, we derive an ellipsoid that has a ratio of its minor to major axes of $0.65 \leq b/a \leq 0.73$. This is similar to that of DQ Her (see below), suggesting that interaction with the accretion disk and/or secondary star acts to slow the progress of the ejecta in the plane of the binary star system.

4.2. DQ Herculis

DQ Her erupted in 1934, reaching maximum on 22 December. Monographs by McLaughlin (1937) and Beer (1974) thoroughly discuss the spectroscopy of the outburst of this prototypical dust-producing nova. DQ Her is classified as a moderate speed nova, and we tabulate the means of the decline rates taken from the literature (McLaughlin 1939, Strope et al. 2010, Duerbeck 1987) in Table 4. In addition to those published values, we have examined the light curve data published by Gaposchkin (1956) and the light curve assembled by Beer (1974), to derive additional values of $t_2 = 80.4$ d, 67 d, and $t_3 = 94.3$ d, 94 d, respectively, and these data been incorporated into the means listed in the Table 4. Downes & Duerbeck (2000) list $t_2 = 39$ d for DQ Her, but this value is due to a short-lived dip at the end of 1935 March, from which the nova recovered, after which it resumed the more general decline rate that was present before this event. We have not incorporated that value into the t_2 mean for DQ Her.

The published data for the light curve maxima are all quite similar and lead to the mean of $v_{\max} = 1.3$ listed in Table 4. The value of the visual extinction to DQ Her is somewhat more uncertain. The commonly quoted value is $A_V = 0.35$, but this appears to be due to the value quoted in Ferland et al. (1984). Ferland et al. state that this value is the line-of-sight extinction for galaxies in this direction from de Vaucouleurs et al. (1976). Analysis of *IUE* spectra of DQ Her by Verbunt (1987) gives a similar value for the extinction: $E(B - V) = 0.1$. As shown in Fig. 1, if we use this value, DQ Her has a significantly higher extinction than its reference frame stars. The IRSA data base gives a much lower value of $A_V = 0.13$ for the line-of-sight extinction at the location of DQ Her. This latter estimate is perfectly consistent with the values we derived for the astrometric reference frame stars. We find that DQ Her appears to suffer from an anomalously high extinction. The most likely explanation is excess *local* extinction from circumstellar material, perhaps from the dust shell created in the eruption. Note that Evans (1991) detected molecular gas around this object, and DQ Her was also detected at both 60 and 100 μm by *IRAS* (Harrison & Gehrz 1988, Callus et al. 1987, Dinerstein 1986).

To determine the absolute visual magnitude of DQ Her at outburst maximum, we have incorporated the value of $A_V = 0.31$ from Verbunt (1987). With $d = 386$ pc and $v_{\max} = 1.3$, this leads to $M_{V_{\max}} = -6.94$. If the excess extinction is due to the dust shell created in April of 1935, however, DQ was slightly fainter (0.18 mag) at visual maximum: $M_{V_{\max}} = -6.76$. This shows that at its peak, assuming $M_1 = 0.60 \pm 0.07 M_\odot$ (Horne et al. 1993), the luminosity of DQ Her exceeded the Eddington limit by about 0.7 mag.

Vaytet et al. (2007) provide the most recent analysis of the size and structure of DQ Her's ellipsoidal ejected shell, including the detection of clumps/knots that appear to be ablated by a strong stellar wind aligned with the poles of the binary. They find the radial distances to the center of the ring of the ejected shell in the major and minor axis directions

to be $a = 25.31 \pm 0.44$, and $b = 18.70 \pm 0.44$ arcseconds, respectively (epoch 1997.82). They derived a maximum line-of-sight velocity of 370 km s^{-1} , from which they calculated a distance of $525 \text{ pc} \pm 28 \text{ pc}$. This number is substantially larger than our astrometric value.

If we use the new parallax and the Vaytet et al. measurements, we derive expansion velocities of 368 and 272 km s^{-1} along the major and minor axes, respectively. The mean of these two velocities (320 km s^{-1}) is very close to the value of the velocity of the principal absorption component listed by McLaughlin (1940): 315 km s^{-1} . Ferland (1980) quote that analysis of the emission lines from the nebular shell gave a velocity of $320 \pm 20 \text{ km s}^{-1}$. While the average of the velocities of the two shell axes is consistent with the assumption that the principal velocity component observed near maximum light is associated with the bulk of the ejecta for DQ Her, the details are not.

We plot the values for the expanding shell of DQ Her in Fig. 4. The early micrometer measures by Kuiper (1941) are only of the major axis. The first measure of the minor axis dimension is due to Baade (1940). Duerbeck (1987) tabulates the measures up to 1984. The last three measurements plotted in Fig. 4 are due to Slavin et al. (1995), Vaytet et al. (2007), and our own measurement of an unpublished *HST* WFPC2 image (*HST* Proposal ID: 6060) obtained on 1995 September 4. As shown in Fig. 4, the diameter of the major axis of the nebula suggests an expansion velocity in excess of 320 km s^{-1} , while the minor axis of the nebula is much smaller than would be expected if it was expanding at this rate. In fact, these data are suggestive of a slowing in the rate of expansion of the minor axis that appears to have started around 1970, when the shell’s distance from the central binary was $\sim 1.7 \times 10^{16} \text{ cm}$. This suggests to us that there is pre-existing material into which the ejected shell has collided that has acted to retard its progress. Perhaps this is evidence for a circumbinary disk of material (c.f., Dubus et al. 2002). DQ Her is an eclipsing binary, and we view the system almost edge on: $i = 86.^{\circ}5$ (Horne et al. 1993), and thus circumbinary

material along the minor axis would be aligned with the plane of the underlying binary. Such a structure could also be responsible for the excess extinction, the *IRAS* detections, and the H₂ emission.

4.3. GK Persei

The first bright nova of the twentieth century was discovered on 1901 February 21 by T. D. Anderson. Campbell (1903) compiled the light curve data for GK Per, and concluded that it reached a visual maximum of $m_{v,\text{max}} = 0.2$ on February 23rd. However, there are six estimates in Campbell’s Table II that are brighter than his quoted peak for this nova. It is unclear why those data were ignored, as they come from respected observers: E. C. Pickering, W. H. Pickering, and A. J. Cannon. In the cases of these three observers, they all quoted GK Per as being “two grades” (0.2 mag) brighter than Capella ($V = 0.08$). Fortunately, for much of the data set, Campbell lists the actual brightness estimates relative to various comparison stars, and we can use modern values for the V magnitudes of the comparison stars to regenerate the light curve of GK Per. We plot these “calibrated” magnitudes for GK Per in Fig. 5 as solid circles. If the comparison stars were not listed, the magnitudes in Campbell’s Table II were used and are plotted as crosses in Fig. 5. Clearly, GK Per was at least as bright as $V = 0.0$ at maximum. This is the value quoted by Humason (1938) in his tabulation of novae maxima, and is what we have listed in Table 4. Additional support for this result is found in the popular literature of the time: “On February 22, 1901, a marvelous new star was discovered by Doctor Anderson of Edinburgh, not very far from Algol. No star had been visible at that point before. Within twenty-four hours the stranger had become so bright that it outshone Capella. In a week or two it had visibly faded, and in the course of a few months it was hardly discernible with the naked eye.” (G. P. Serviss, as quoted by Lovecraft, 1919).

The initial decline of GK Per from maximum was very smooth, and the mean values for t_2 and t_3 have small error bars. The extinction to GK Per, however, is quite large: $A_V = 0.96$ mag (averaging the values from Wu et al. 1989, and Shara et al. 2012). With $d = 477$ pc, this leads to $M_{V_{\max}} = -9.35$. As noted above, it is quite possible that GK Per was 0.1 mag more luminous than this at the time of visual maximum.

The structure of the shell of GK Per has been extensively investigated by Seaquist et al. (1989) and Shara et al. (2012). Slavin et al. (1995) reported that the shell had dimensions of $103'' \times 90''$ on 1993 September 10. With the parallax, those dimensions correspond to expansion velocities of 1,256 and 1,100 km s⁻¹ for the major and minor axes, respectively. McLaughlin (1940) lists the principal absorption component of GK Per having a velocity of $v_{\text{principal}} = 1,300$ km s⁻¹, similar to that derived for the major axis. The nebula ejected by GK Per is asymmetric and Seaquist et al. discuss a scenario where the nova erupted within a circumstellar cloud that is several parsecs across, with which it is now interacting. They propose it is this material that was responsible for the light echos observed following outburst (c.f., Perrine 1902).

GK Per is an unusual CNe, having the second longest orbital period known: 1.9968 d (Morales-Reuda et al. 2002). Clearly, the secondary star must be substantially larger than a main sequence star to fill its Roche lobe and transfer matter to the white dwarf primary. We can use the new distance and the implied Roche lobe geometry to investigate the nature of this system. Sherrington & Jameson (1983) list GK Per as having $K = 10.14$ at minimum light. As shown in Harrison et al. (2007), the K2 secondary star of GK Per completely dominates the spectral energy distribution in the near-infrared. This leads to $M_K = 1.65$ for the subgiant secondary star. A K2V has $M_K = 4.15$, thus the secondary star in GK Per is exactly ten times more luminous than its main sequence counterpart. If we compare the secondary star of GK Per to the K2 dwarf ϵ Eridani ($R = 0.74 \pm 0.01 R_\odot$, Baines &

Armstrong 2012), we calculate that its mean radius is $R_2 = 1.63 \times 10^{11}$ cm. Using the relationships in Warner (1995) between the orbital period, semi-major axis, the mass ratio ($q = 0.55 \pm 0.21$; Morales-Reuda et al. 2002), and the Roche lobe radius of the secondary star, we derive that the white dwarf in GK Per has a mass of $M_1 = 0.77_{-0.24}^{+0.52} M_\odot$ (where the limits on the mass only contain the errors associated with q). This simple calculation shows that the mass of the white dwarf in GK Per is not unusual when compared to other CVs (see Cropper et al. 1998), though a new study to refine the value of the mass ratio is clearly warranted. If we assume that the bolometric correction at visual maximum is zero, then for the derived white dwarf mass, GK Per exceeded the Eddington luminosity by a factor of fourteen at its peak, and remained above this limit for at least 10 days.

4.4. RR Pictoris

RR Pic was a very slow nova that erupted in 1925. A light curve of its outburst can be found in Spencer Jones (1931), in which visual maximum occurs on 7 June, 1925. We have compiled the t_2 and t_3 decline rates from the literature (Downes & Duerbeck 2000; McLaughlin 1939; Duerbeck 1987; and Strope et al. 2010), and to those we add the values of $t_2 = 82$ d and $t_3 = 122$ d from our analysis of the light curve compiled by Campbell (1929), to construct the mean values listed in Table 4. Spencer Jones notes the unusual behavior of this object, in that it was later found on patrol photographs to be at $m_v = 3.0$ some six weeks prior to discovery. Spencer Jones also notes that an amateur stated that he was confident that no new naked eye stars were present at this position only four days prior to discovery. Given that there was a two month gap between the patrol photographs showing it to clearly be at minimum (18 February), and the pre-discovery observation, Spencer Jones suggests that perhaps the true visual maximum of this object was missed, and the maximum that occurred in June of that year was a secondary event.

The line-of-sight extinction to RR Pic is low, with the mean of the published values (Verbunt 1987; Krautter et al. 1981; Williams & Gallagher 1979) giving $A_V = 0.13$ mag. The mean value of the visual maximum from the light curve sources listed above is $V_{\max} = 1.1 \pm 0.1$; this leads to $M_{V_{\max}} = -7.61$, about 1 mag above the Eddington limit for a $1 M_\odot$ white dwarf. This luminosity is larger than expected given that RR Pic was a slower nova than DQ Her. If maximum absolute visual magnitude is assumed to be directly correlated with the light curve decline rate, RR Pic should have been *less* luminous than DQ Her since it was the slower nova. Instead, RR Pic was almost twice as luminous as DQ Her at their respective peaks. This may be additional evidence that the true visual maximum of this CNe was missed.

McLaughlin (1940) lists the principal component expansion velocity as 285 km s^{-1} , while Payne-Gaposchkin (1957) has $v_{\text{principal}} = 310 \text{ km s}^{-1}$. Both Williams & Gallagher (1979) and Gill & O'Brien (1998) present analyses of the nebular shell of RR Pic. At the epochs of those two observations, a freely expanding spherical shell with $v = 310 \text{ km s}^{-1}$ would have diameters of $13.0'' \pm 1.2''$ and $17.6'' \pm 1.7''$, respectively. The actual shells had dimensions of $23'' \times 18''$ (Williams & Gallagher 1979) and $30'' \times 21''$ (Gill & O'Brien 1998). The observed shells are significantly larger than would be expected if the velocity of the principal absorption component measured near the June maximum was correct. Spencer Jones lists a variety of other velocity systems for RR Pic, but none of them appear to correspond to the velocity ($\sim 430 \text{ km s}^{-1}$) required to create the observed shell sizes.

RR Pic was observed with WFPC2 on the *HST* in 1999 (26 February, Prop. ID #6770). We have analyzed those data and find that the *centers* of the main shell features are separated by $22.7''$. These features are quite diffuse, but appear correspond to the “equatorial ring” condensations visible in the images presented by Gill & O'Brien (1998). To be of this size requires an expansion velocity of 380 km s^{-1} . While this is closer to the

observed principal velocity than implied by the previous studies, its remains 20% larger. Note that even the first visual micrometer observations of the young shell (van den Bos & Finsen 1931) are consistent with this higher than expected ejecta velocity. Unlike the results for the previous objects, it is not as obvious why the nebular expansion parallax method fails for RR Pic.

5. Discussion

To fully understand the outbursts of CNe, we need to have precise distances to accurately calorimeter their outbursts, and to allow us to examine the shell ejection process. Theory suggests that fast novae occur on massive white dwarfs, have the most luminous outbursts, have light curves exhibit the most rapid decline rates, and their ejecta have the highest expansion velocities. While our sample is tiny, having precise parallaxes for four objects sheds new light into the difficulties of making broad assumptions about the behavior of CNe.

In Fig. 6 we have plotted the absolute magnitudes at visual maximum ($M_{V_{\max}}$) versus the *log* of their light curve decline rates (both t_2 and t_3) for the four program CNe. We also plot the various MMRD relationships discussed in Downes & Duerbeck (2000). Both GK Per and DQ Her fall very close to the linear relationships for t_2 and t_3 . While the older “arctangent” law of Della Valle & Livio (1995) works for both V603 Aql and DQ Her. RR Pic remains an outlier in all cases. As Downes & Duerbeck show, there remains a scatter of ~ 0.5 mag around the various relationships, and it was hoped that those inaccuracies were due to flaws in the secondary distance estimation techniques. The astrometric results show that such discrepancies remain.

We believe, however, that there are possible (partial) explanations for why both RR

Pic and V603 Aql are so discrepant. For RR Pic, there appears to be sufficient evidence to suggest that the 1925 June 6 maximum was a secondary event. If one presumes the initial maximum reached to the same level as the June maximum ($m_v = 1.1$), then if it erupted sometime after 1925 February 18 (the last quiescent patrol photograph), and was third magnitude on 1925 April 13, then it would have had $t_2 \leq 54$ d. This moves it much closer to the linear relationship for t_2 (it needs to have $t_2 = 29$ d to fall on exactly the line). There have been a number of CNe that have been observed to have complex light curves similar to that needed to have been exhibited by RR Pic to reconcile its decline rate with its observed absolute magnitude (see the “C-class”, and “J-class” CNe light curves in Strope et al. 2010). The main difficulty with this scenario is that it is hard to believe that a first magnitude nova would have escaped detection, given that it was reasonably well placed for evening viewing in March and April.

While V603 Aql does fall near the older arctangent law, its outburst was quite underluminous for the speed class when compared to the two linear laws. We argued above that the data suggests V603 Aql exceeded the commonly tabulated value of $m_{V_{\max}} = -1.1$, probably reaching $m_{V_{\max}} = -1.4$. The question was whether it was even brighter than this. To get the absolute visual magnitude to fall closer to the linear law lines, V603 Aql would have had to have reached $m_{V_{\max}} \approx -2.4$. There is a seven hour gap in the light curve right at the time of visual maximum, so it is quite possible that the true maximum was missed. But an extrapolation of the rise to the observed maximum suggests that it would have required a sudden change in slope to exceed $m_{V_{\max}} \approx -1.8$. Thus, there truly appears to be a difference between the absolute visual magnitudes at maximum of V603 Aql and GK Per, even though their light curve decay rates were quite similar. Given that the principal ejecta velocities were higher for V603 Aql, suggests that it had the more violent eruption. This implies that there must be another parameter besides white dwarf mass that acts to govern the luminosity of CNe outbursts. The fact that the nebular remnant of GK Per is

still visible more than 100 yr after outburst, while that of the more recent V603 Aql is not, indicates that the shells ejected by these two objects were quite different.

Downes & Duerbeck (2000) also explore the suggestion (originally due to Buscombe & de Vaucouleurs 1955) that all CNe have the same absolute visual magnitudes 15 days after visual maximum, finding $M_{V,t=15d} = -6.04$. Using the published light curves we find that there is more than a 1.5 mag spread between V603 Aql ($M_{V,t=15d} = -4.4$) and GK Per ($M_{V,t=15d} = -6.0$) at this time in their outbursts. We conclude that using the decline rates of CNe light curves to obtain reliable distances is not possible. The fastest, and therefore most luminous novae, need near constant photometric monitoring to fully constrain their peak brightnesses. Even then, there are intrinsic differences in their outbursts that limits their value as standard candles.

While CNe may not be the best objects to use for extragalactic distance estimates, the question is whether we can actually determine the distances to individual CNe to attempt to characterize their outbursts. The most reliable secondary distance estimation technique we have is the nebular expansion parallax method. This technique remains the main source of distances to CNe, and has been used to calibrate the various MMRD relationships. The news on this front is also not very heartening. For V603 Aql, we found that the velocity of the principal absorption component ($1,500 \leq v_{\text{principal}} \leq 1,700 \text{ km s}^{-1}$) was much higher than the observed expansion rate of the ejecta: $1,100 \text{ km s}^{-1}$. For DQ Her, the results were slightly better, except it appears that the expansion rate of the ejecta in the plane of the binary (the minor axis of the nebula) has slowed over the last 40 years. For RR Pic, the nebula is expanding much more rapidly than than the derived $v_{\text{principal}}$. Only for GK Per is the expansion parallax in accordance with expectations.

The good news is that we believe we can resolve the discrepancies for the three discordant CNe. The smaller than expected expansion of the shells of DQ Her and V603 Aql

appears to be due to the interaction of the ejecta with the secondary star or with material that lies within the plane of the underlying binary star orbit. Note that we calculated that V603 Aql and DQ Her appear to have similar ratios of the minor to major axes for their ellipsoidal shells. Unfortunately, to determine this requires one to construct a model for each of these shells, stressing the importance of high resolution spectroscopy throughout the outburst and decline of CNe, as well as follow-up, multi-epoch imaging. For RR Pic, the discrepancy can be eliminated if we assume that the observed maximum was in fact a secondary maximum. This simply requires a slightly higher principal ejecta velocity at the time of its true maximum.

Lloyd et al. (1997) have simulated the effect that the underlying binary has in shaping the shells of CNe. The results from Lloyd et al. suggest that the shells of fast novae should mostly ignore the underlying binary. But this is not the case for V603 Aql. It appears that the shell of V603 Aql was as non-spherical as that of the much slower DQ Her. All three of the CNe for which the nebular expansion parallax technique does not work have much shorter orbital periods ($P_{\text{DQ}} = 4.64$ hr, $P_{\text{RR}} = 3.48$ hr, $P_{\text{V603}} = 3.32$ hr) than for the concordant GK Per ($P_{\text{GK}} = 48.1$ hr). This suggests to us that the interaction of the secondary star with the ejecta is probably more important than the simulations indicate.

One of the unfortunate aspects of the current CNe sample is that three of the objects have been classified as “Intermediate Polars”, CVs that are believed to have highly magnetic white dwarf primaries ($B \lesssim 1$ MG). Such objects are identified by having coherent periodicities that are shorter than their orbital periods, assumed to originate from processes occurring at the magnetic poles of the rapidly rotating white dwarfs in these systems. It is unclear if strong magnetic fields play any role in shaping the outburst or the ejecta of CNe (Livio et al. 1988, Nikitin et al. 2000). The fact that RR Pic is not an Intermediate Polar (Pekön & Balman 2008), but also has a discrepant nebular expansion parallax, indicates

that the presence of a strong magnetic field does not appear to dramatically affect the shell ejection process.

The luminosities of the outbursts of CNe are obviously more complex than being a simple function of the mass of the white dwarf primary in the underlying binary. It would be extremely useful to have additional parallaxes to construct a larger sample of objects with precise distances but, unfortunately, few CNe have minimum magnitudes that will allow for precise parallaxes even with the *GAIA* mission. The subset of those that had outbursts with the quality of data necessary to deconvolve the nature of their outbursts is even smaller. Thus, progress on characterizing CNe outbursts will be better served by observations of future CNe. This will require more thorough all-sky monitoring to insure that the light curves of these objects have better temporal coverage. In addition, however, multi-epoch interferometric, high resolution imaging, and moderate resolution spectroscopic observations of these CNe will also be required.

Support for program AR12617 was provided by NASA through a grant from the Space Telescope Science Institute, which is operated by the Association of Universities for Research in Astronomy, Inc., under NASA contract NAS 5-26555.

References

- Arenas, J., Catalán, M. S., Augusteijn, T., & Retter, A. 2000, MNRAS, 311, 135
Baade, W. 1940, PASP, 52, 386
Baines, E. K., & Armstrong, J. T., 2012, ApJ, 744, 138
Barnard, E. E. 1919, ApJ, 49, 199
Beer, A. 1974, Vistas in Astronomy, 16, 179
Benedict, G. F., et al. 2011, AJ, 142, 187
Benedict, G. F., McArthur, B. E., Bean, J. L., Barnes, R., Harrison, T. E., Hatzes, A.,

- Martioli, E., & Nelan, E. P. 2010, AJ, 139, 1844
- Benedict, G. F., McArthur, B. E., Feast, M. W., Barnes, R., Harrison, T. E., Patterson, R. J., Menzies, J. W., Bean, J. L., & Freedman, W. L. 2007, AJ, 133, 1810
- Benedict, G. F. et al. 2002b, AJ, 124, 1695
- Benedict, G. F. et al. 2002a, AJ, 123, 473
- Bruch, A., & Engel, A. 1994, A&AS, 104, 79
- Buscombe, W., & de Vaucouleurs, G. 1955, Observatory, 75, 170
- Callus, C. M., Evans, A., Albinson, J. S., Mitchell, R. M., Bode, M. F., Jameson, R. F., King, A. R., & Sherrington, M. 1987, MNRAS, 229, 539
- Campbell, L. 1929, Harvard Bull., 835
- Campbell, L. 1919, Harvard Ann., 81, 113
- Campbell, L. 1903, Harvard Ann., 48, 39
- Cannizzo, J. K., Still, M. D., Howell, S. B., Wood, M. A., & Smale, A. P. 2010, ApJ, 725, 1393
- Conroy, C. C. 1918, MNRAS, 79, 37
- Cox, A. N. 2000, “Allen’s Astrophysical Quantities”, (AIP Press: New York)
- Cropper, M., Ramsay, G., & Wu, K. 1998, MNRAS, 293, 222
- de Vaucouleurs, G., de Vaucouleurs, A., & Corwin, J. R. 1976, in *Second reference catalogue of bright galaxies*, (Austin: University of Texas Press)
- Della Valle, M., & Gilmozzi, R. 2002, 296, 1275
- Della Valle, M., & Livio, M. 1995, ApJ, 452, 704
- Dinerstein, H. L. 1986, AJ, 92, 1381
- Downes, R. A., & Duerbeck, H. W. 2000, AJ, 120, 2007
- Ferland, G. J., Williams, R. E., Lambert, D. L., Shields, G. A., Slovak, M., & Gondhalekar, P. M. 1984, ApJ, 281, 194
- Ferland, G. J., 1980, The Observatory, 100, 166

- Gill, C. D., & O'Brien, T. J. 1998, MNRAS, 300, 221
- Hachisu, I., & Kato, M. 2010, ApJ, 709, 680
- Hanson, R. B. 1979, MNRAS, 186, 875
- Harrison, T. E., Johnson, J. J., McArthur, B. E., Benedict, G. F., Szkody, P., Howell, S. B., & Gelino, D. M. 2004, 127, 460
- Harrison, T. E., & Gehrz, R. D. 1988, AJ, 96, 1001
- Holtzman, J. A., Harrison, T. E., Coughlin, J. L. 2010, Adv. Astron., 193086
- Horne, K., Welsh, W. F., & Wade, R. A. 1993, ApJ, 410, 357
- Houk, N., Swift, C. M., Murray, C. A., Penston, M. J., & Binney, J. J. 1997, in Proc. ESA Symposium on HipparcosVenice 1997 (ESA SP-402; Noordwijk: ESA), 279
- Humason, M. L. 1938, ApJ, 88, 228
- Jefferys, W. H., Fitzpatrick, M. J., & McArthur, B. E. 1988, Celest. Mech., 41, 39
- Krautter, J., Vogt, N., Lare, G., Wolf, B., Duerbeck, H. W., Rahe, J., & Wargau, W. 1981, A&A, 102, 337
- Kuiper, G. P. 1941, PASP, 53, 330
- Livio, M., Shankar, A., & Truran, J. W. 1988, ApJ, 330, 264
- Lloyd, H. M., O'Brien, T. J., & Bode, M. F. 1997, MNRAS, 284, 137
- Lovecraft, H. P. 1919, in “Beyond the Wall of Sleep”, *Pine Cones*, 1, 2
- Lutz, T. E., & Kelker, D. H. 1973, PASP, 85, 573
- McArthur, B. E., et al. 2002, in “The 2002 HST Calibration Workshop: Hubble after the Installation of the ACS and the NICMOS Cooling System, ed. S. Arribas, A. Koekemoer, & B. Whitmore (Baltimore: Space Telescope Science Institute), 373
- McArthur, B. E., et al. 2001, ApJ, 560, 907
- McLaughlin, D. B. 1945, PASP, 57, 69
- McLaughlin, D. B. 1940, ApJ, 91, 369
- McLaughlin, D. B. 1939, Popular Astronomy, 47, 410

- McLaughlin, D. B. 1937, *Publ. Obs. Univ. Mich.*, 6, No. 12, 107
- Morales-Rueda, L., Still, M. D., Roche, P., Wood, J. H., & Lockley, J. J. 2002, MNRAS, 329, 597
- Nelan, E., et al. 2011, “Fine Guidance Sensor Instrument Handbook”, Version 19.0, (Balitmore: STScI)
- Nikitin, S. A., Vshivkov, V. A., & Snytnikov, V. N. 2000, Astronomy Letters, 26, 362
- O’Brien, T. J., & Bode, M. F. 2008, in “Classical Novae”, ed. M. F. Bode and A. Evans (Cambridge University Press: New York), p285
- Payne-Gaposchkin, C. 1957, *The Galactic Novae* (Dover, New York)
- Pekön, Y., & Balman, §. 2008, MNRAS, 388, 921
- Perrine, C. D. 1902, ApJ, 14, 249
- Perryman, M. A. C., et al. 1997, A&A, 323, 49
- Rieke, G. H., Lebofsky, M. J. 1985, ApJ, 288, 618
- Roeser, S., Demleitner, M., & Schilbach, E. 2010, AJ, 139, 2440
- Seaquist, E. R., Bode, M. F., Frail, D. A., Roberts, J. A., Evans, A., & Albinson, J. S. 1989, ApJ, 344, 805
- Shara, M. M., Zurek, D., De Marco, O., Mizusawa, T., Williams, R., & Livio, M. 2012, ApJ, 143, 143
- Sherrington, M. R., & Jameson, R. F., 1983, MNRAS, 205, 265
- Soderblom, D. R., Nelan, E., Benedict, G. G., McArthur, B., Ramirez, I., Spiesman, W., & Jones, B. F. 2005, AJ, 129, 1616
- Spencer Jones, H. 1931, Cape Ann., 10, 9
- Standish, E. M. Jr. 1990, A&A, 233, 252
- Starrfield, S., Iliadis, C., Hix, W. R., Timmes, F. X., & Sparks, W. M. 2009, ApJ, 692, 1532
- Strope, R. J., Schaefer, B. E., & Henden, A. A. 2010, ApJ, 140, 34
- Townsley, D. M., & Bildsten, L. 2004, ApJ, 600, 390

- van den Bos, W. H., & Finsen, W. S. 1931, MNRAS, 92, 19
- van den Bergh, & Pritchett, C. J. 1986, PASP, 98, 110
- van Leeuwen, F. 2007, in “Hipparcos, the new reduction of the raw data (Dordrecht: Springer)
- Verbunt, F. 1987, A&A Supp., 71, 339
- Wade, R. A., Harlow, J. J. B., & Ciardullo, R. 2000, PASP, 112, 614
- Warner, B. 2008, in “Classical Novae”, ed. M. F. Bode and A. Evans (Cambridge University Press: New York), p16
- Weaver, H. 1974, in Contopolous G., ed., Highlights of Astronomy, Vol. 3., (Reidel: Dordrecht), p. 509
- Williams, R. E., & Gallagher, J. S. 1979, ApJ, 228, 482
- Wu, C. -C., Holm, A. V., Panek, R. J., Raymond, J. C., Harmann, L. W., & Swank, J. H. 1989, ApJ, 339, 443
- Wyse, A. B. 1940, Pub. Lick. Obs., 14, 93
- Yamashita, Y., Nariai, K., & Normoto, Y. 1978, “An Atlas of Representative Stellar Spectra”, (Halsted Press: New York)

Table 1. Astrometric Reference Stars^a

ID	α_{2000}	δ_{2000}	μ_α (mas yr $^{-1}$)	μ_δ (mas yr $^{-1}$)	Sp. Ty.	V	(B – V)	A _V	π (mas) ^b
V603 Aql R01	18:49:19.30	+00:34:26.30	0.40±0.244	-21.81±0.17	G2V	13.36	1.05	1.39	3.28±0.13
V603 Aql R02	18:49:01.90	+00:33:46.40	-9.48±0.39	-30.17±0.23	K5V	13.62	1.16	0.29	6.76±0.25
V603 Aql R03	18:48:48.20	+00:34:59.80	3.13±0.19	-4.59±0.20	F0V	15.78	1.45	3.16	0.90±0.05
V603 Aql R04	18:48:46.30	+00:35:50.60	4.95±0.15	-7.97±0.16	K2III	14.17	2.31	3.56	0.92±0.05
V603 Aql R05	18:48:41.00	+00:38:49.50	6.45±0.32	-7.45±0.25	F0V	9.88	0.39	0.29	3.56±0.15
V603 Aql R06	18:48:49.50	+00:38:26.80	25.18±0.43	-26.84±0.43	K0V	12.43	0.82	0.00	4.79±0.24
V603 Aql R07	18:48:55.80	+00:36:28.80	-2.31±0.22	-4.60±0.21	K5III	15.38	2.26	2.32	0.23±0.01
V603 Aql R08	18:48:53.00	+00:36:18.20	2.79±0.18	-0.29±0.20	K0V	14.98	1.02	0.91	2.48±0.167
V603 Aql R09	18:49:00.79	+00:36:37.60	-3.59±0.33	-0.64±0.27	B0V	15.00	1.70	6.20	0.27±0.01
DQ Her R01 ^c	18:07:38.42	+45:47:35.40	2.50±0.15	-3.37±0.17	F2V	10.80	0.52	0.10	1.82±0.15
DQ Her R02	18:07:33.18	+45:47:30.60	-5.32±0.33	7.68±0.38	G1V	13.05	0.66	0.05	1.87±0.20
DQ Her R03	18:07:26.70	+45:47:57.50	-3.24±0.37	-3.54±0.32	K3III	11.57	0.66	0.14	0.63±0.07
DQ Her R04	18:07:23.90	+45:49:47.60	-13.87±0.34	-13.26±0.36	G2V	14.23	0.66	0.10	1.20±0.11
DQ Her R05	18:07:29.97	+45:49:49.70	3.34±0.33	-8.13±0.38	G0V	15.12	0.63	0.11	0.70±0.06
DQ Her R06	18:07:20.44	+45:51:14.80	-12.64±0.35	-25.45±0.41	K4V	14.30	1.10	0.10	3.78±0.27
DQ Her R07	18:07:17.75	+45:52:53.70	-0.79±0.31	6.58±0.35	G2V	14.65	0.63	0.13	0.93±0.14
DQ Her R08	18:07:25.45	+45:54:06.50	-4.18±0.32	-16.21±0.35	G2V	14.35	0.67	0.13	1.28±0.14
DQ Her R09	18:07:13.60	+45:55:26.60	-10.00±0.30	-4.91±0.34	F8V	12.71	0.58	0.09	1.59±0.18

^aThe α_{2000} and δ_{2000} are GSC2 coordinates and have the following epochs: V603 Aql = 1990.63, DQ Her = 1991.68, GK Per = 1989.76, and RR Pic = 1995.07.

^bAs noted in the text, the error bars on the reference star parallaxes listed here result from astrometric solutions to the various FGS data sets, and are not independent measurements. For distant reference stars, the final errors on the parallaxes reported by the astrometric solution are more heavily weighted by those of the input spectroscopic parallaxes. For nearer stars, the error in the parallaxes are more heavily weighted by the positional uncertainty of the FGS measurements. An example of the latter is V603 Aql R02. The input spectroscopic parallax for this star was 6.71 ± 1.4 mas. The error bar on the spectroscopic parallax for V603 Aql R02 is larger than the typical positional precision possible with the FGS. Thus, the final error bar on the parallax from the astrometric solution for this nearby star is dominated by the precision of the FGS measurements. In contrast, for a distant reference star such as V603 Aql R07, the error on the input spectroscopic parallax was smaller than that of the intrinsic measurement error of the FGS. Thus, for this star, GaussFit assigns a higher weight to the input spectroscopic parallax.

^cThe spectroscopic parallax for this object is $\pi = 3.02$ mas, but the astrometric solution suggests that it is further away: $\pi = 1.85$ mas. It is quite likely that this is an unresolved binary star with both components having similar spectral types.

Table 1. Astrometric Reference Stars (cont.)

ID	α_{2000}	δ_{2000}	μ_α (mas yr $^{-1}$)	μ_δ (mas yr $^{-1}$)	Sp. Ty.	V	(B – V)	A _V	π (mas)
GK Per R01	03:31:14.18	+43:54:24.60	54.17±0.35	-4.36±0.36	M0V	15.29	1.38	0.0	3.53±0.19
GK Per R02	03:31:24.08	+43:54:43.40	1.78±0.34	-1.39±0.31	F5V	14.49	0.69	0.85	0.87±0.06
GK Per R04	03:31:22.38	+43:55:26.40	-1.84±0.30	-24.83±0.24	G6V	14.84	1.04	1.32	2.07±0.12
GK Per R07	03:31:32.48	+43:55:52.10	10.45±0.16	-15.32±0.16	F7V	13.18	0.75	1.08	2.12±0.10
GK Per R08	03:31:03.99	+43:53:19.70	-1.86±0.25	-13.14±0.24	K1IV	15.78	1.21	0.92	1.87±0.11
RR Pic R01	06:36:27.60	-62:39:04.80	-16.34±0.48	13.77±0.44	G1V	12.27	0.60	0.00	2.66±0.22
RR Pic R03	06:36:07.26	-62:39:34.80	-8.08±0.77	3.24±0.77	G1V	14.71	0.76	0.18	0.89±0.07
RR Pic R04	06:35:51.31	-62:37:46.20	0.29±0.36	11.36±0.38	F5V	13.98	0.63	0.29	0.82±0.07
RR Pic R05	06:35:28.84	-62:38:34.30	-2.46±0.39	15.64±0.31	G2V	15.13	0.88	0.47	0.95±0.07
RR Pic R06	06:35:40.34	-62:38:41.40	1.87±0.51	0.73±0.39	G5V	15.11	0.86	0.22	0.96±0.09
RR Pic R07	06:35:10.83	-62:37:49.10	2.33±0.76	15.45±0.62	G5V	15.22	0.80	0.20	1.00±0.09
RR Pic R08	06:34:57.10	-62:37:11.70	6.16±0.33	12.38±0.30	K0IV	13.93	1.17	0.81	0.84±0.06
RR Pic R09	06:34:50.11	-62:37:40.40	3.12±0.41	6.61±0.36	F6V	15.05	0.61	0.22	0.55±0.05
RR Pic R10	06:35:01.15	-62:38:14.50	1.89±0.76	16.33±0.64	K1.5V	15.28	0.96	0.10	1.82±0.19
RR Pic R11	06:35:07.93	-62:39:53.20	-0.20±0.40	21.07±0.38	G9IV	13.03	0.88	0.26	1.01±0.08
RR Pic R12	06:36:25.98	-62:38:12.50	-3.21±0.27	13.92±0.21	G5III	10.41	0.85	0.17	2.60±0.14

Table 2. Astrometric Properties of Program Classical Novae^c

Nova	α_{2000}	δ_{2000}	μ_α (mas yr $^{-1}$)	μ_δ (mas yr $^{-1}$)	Parallax (mas)	LKH (mag)
V603 Aql	18:48:54.64	+00:35:02.9	11.916 ± 0.142	-10.240 ± 0.131	4.011 ± 0.137	-0.01
DQ Her	18:07:30.26	+45:51:32.1	-2.125 ± 0.210	13.301 ± 0.244	2.594 ± 0.207	-0.05
GK Per	03:31:12.01	+43:54:15.4	-6.015 ± 0.197	-22.767 ± 0.208	2.097 ± 0.116	-0.08
RR Pic	06:35:36.07	-62:38:24.3	5.204 ± 0.222	0.245 ± 0.281	1.920 ± 0.182	-0.07

^cSee footnote *a* for Table 1.

Table 3. Astrometric Distances versus Nebular Expansion Parallax Distances^d

Nova	Astrometric Distance	Nebular Distance
V603 Aql	249^{+9}_{-8}	328^{+60}_{-29}
DQ Her	386^{+33}_{-29}	545^{+81}_{-70}
GK Per	477^{+28}_{-25}	460^{+69}_{-59}
RR Pic	521^{+54}_{-45}	580^{+89}_{-73}

^dFrom Downes & Duerbeck (2000).

Table 4. Outburst Details for Program Classical Novae

Nova	Year of Maximum	t_2	t_3	V_{Max}	$v_{\text{principal}}$	$M_{V_{\text{max}}}$	^e
V603 Aql	1918.764	4.5 ± 0.5	9.3 ± 2.3	$-1.4 \pm 0.3:$	1600	$-8.60_{-0.07}^{+0.08}$	
DQ Her	1934.978	70.0 ± 5.0	95.6 ± 3.0	1.3 ± 0.2	315	$-6.94_{-0.17}^{+0.18}$	
GK Per	1901.148	6.3 ± 0.6	13.0 ± 0.0	0.0 ± 0.1	1200	$-9.35_{-0.11}^{+0.13}$	
RR Pic	1925.436	78.3 ± 4.7	136.0 ± 13.2	1.1 ± 0.1	310	$-7.61_{-0.19}^{+0.22}$	

^eThe errors on these absolute magnitudes represent only the uncertainty due to the parallax, and do not include the uncertainty in V_{Max} .

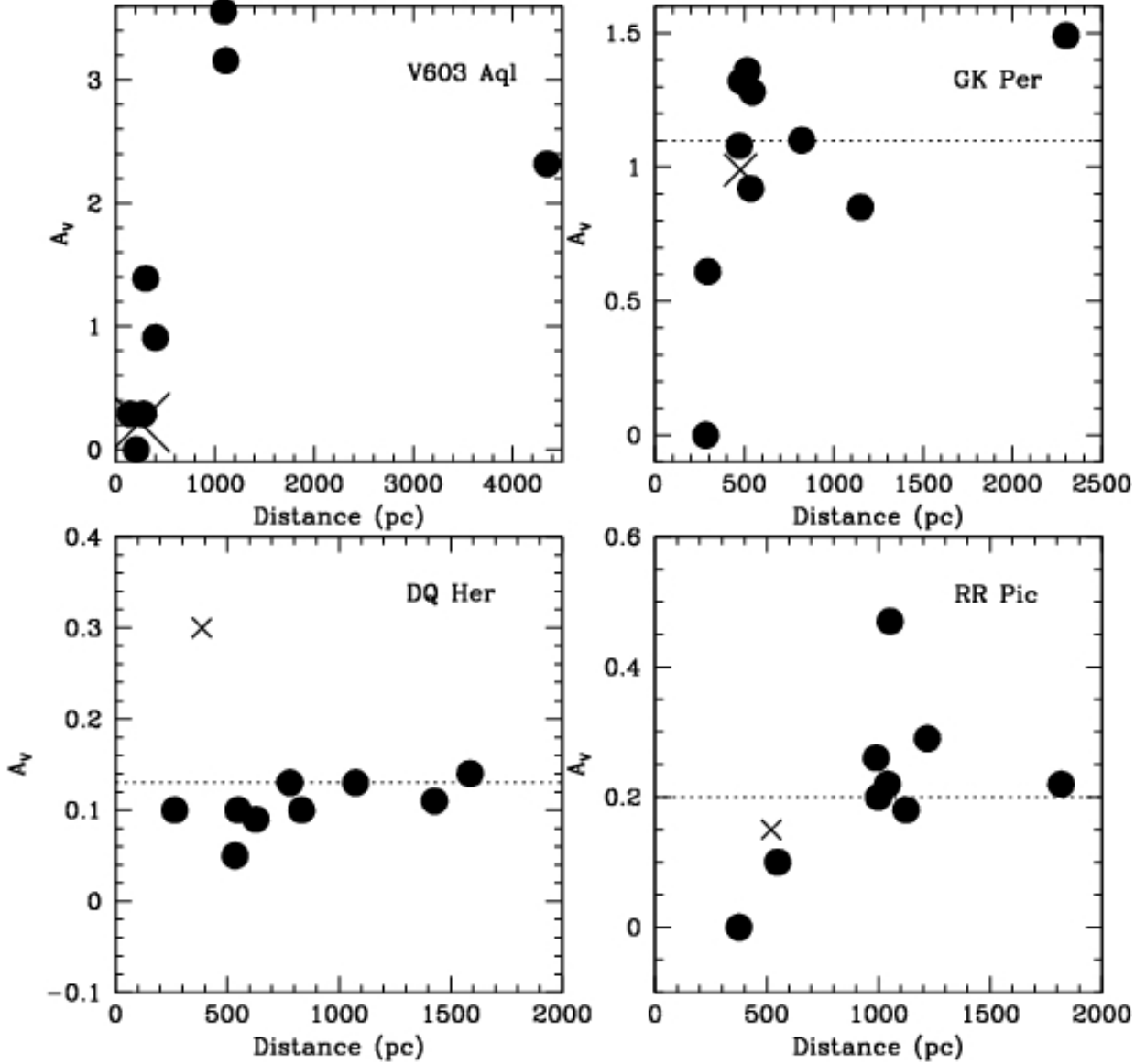


Fig. 1.— The derived extinction of the astrometric reference stars in the four CNe fields versus their distances derived from their spectroscopic parallaxes. The positions of the classical novae are indicated with an “ \times ”. The mean (IRSA) line-of-sight extinction (averaged over a 2° field-of-view) of each field is represented by a horizontal dotted line (except for V603 Aql, where the line-of-sight extinction at its low galactic latitude is $A_V \geq 15$ mag). For GK Per we have plotted our results for all ten of the reference stars, not just the five used in the astrometric solution.

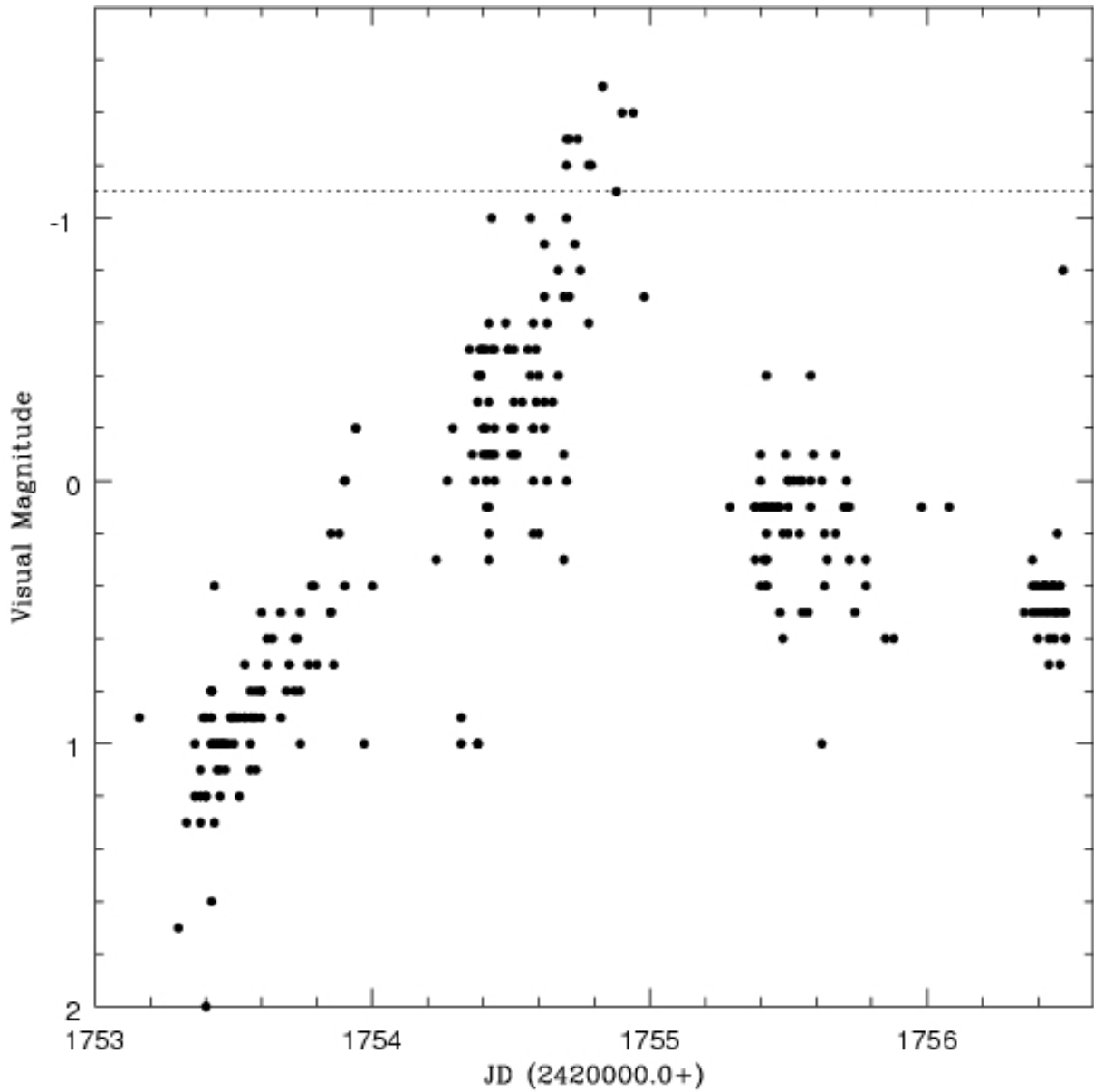


Fig. 2.— The light curve of V603 Aql near visual maximum (Campbell 1919). The dashed line at $m_V = -1.1$ demarcates the commonly quoted value for its visual maximum magnitude.

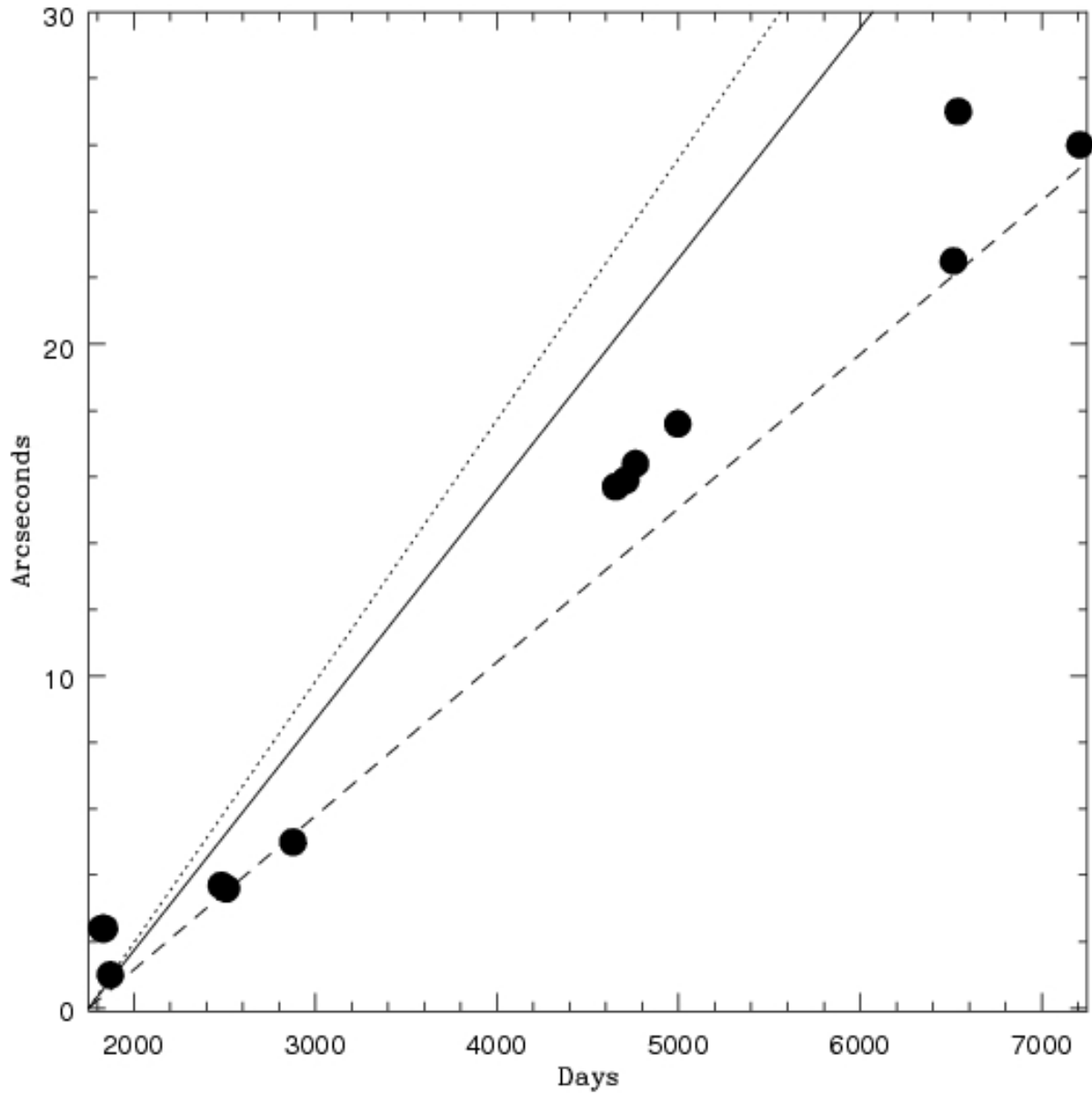


Fig. 3.— The angular expansion rate of the nebular shell of V603 Aql, data (solid circles) from Wyse (1940). The dashed line is the expansion rate if the ejecta velocity was 1,000 km s⁻¹, the solid line is for 1,500 km s⁻¹, and the dotted line is 1,700 km s⁻¹.

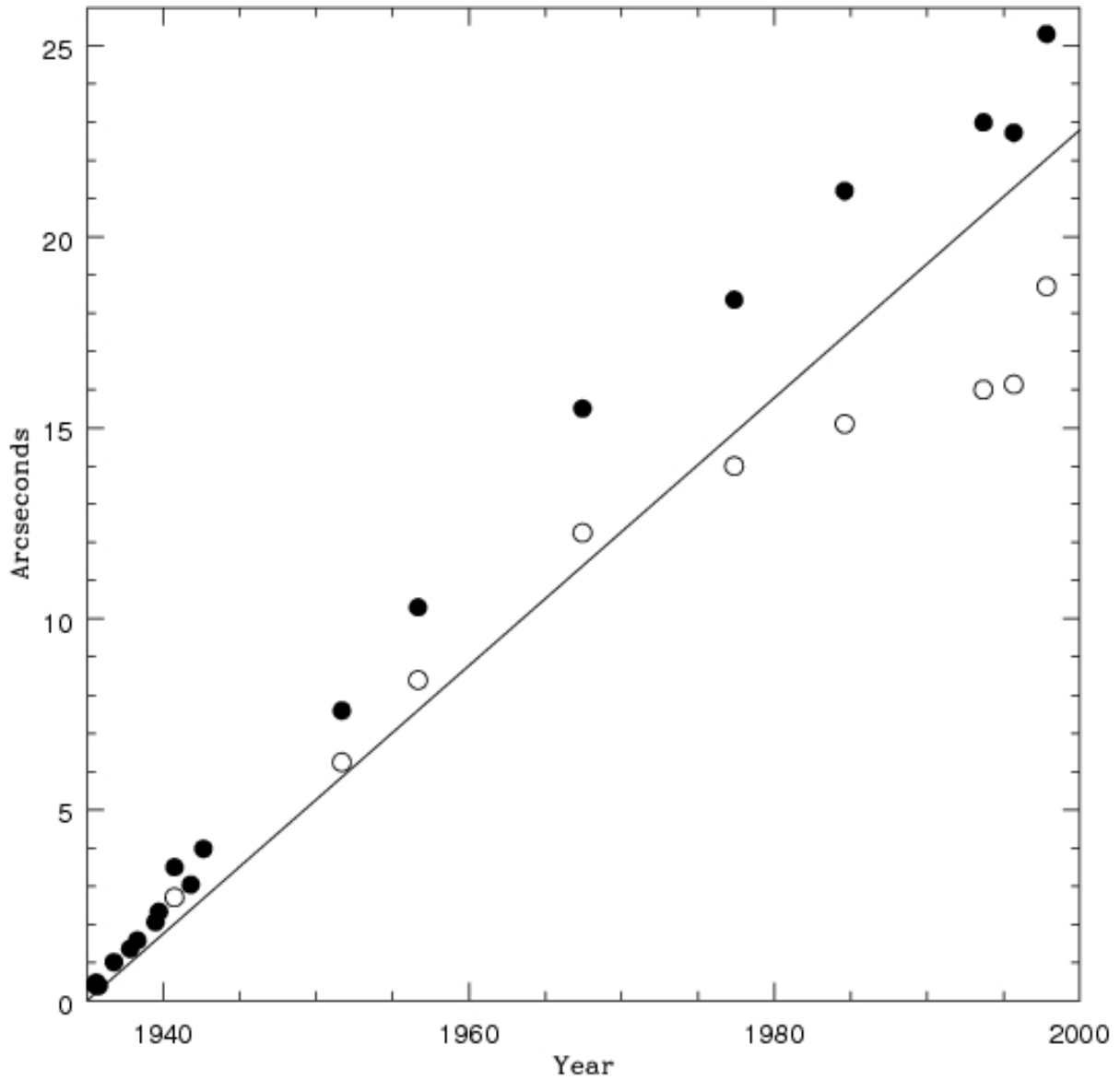


Fig. 4.— The angular expansion rate of the nebular shell of DQ Her. Solid circles are the measurements of the diameter of major axis, while open circles indicate the diameter of the minor axis. The solid line is the projected angular size of a shell that was ejected with $v_{\text{exp}} = 320 \text{ km s}^{-1}$ at the time of outburst.

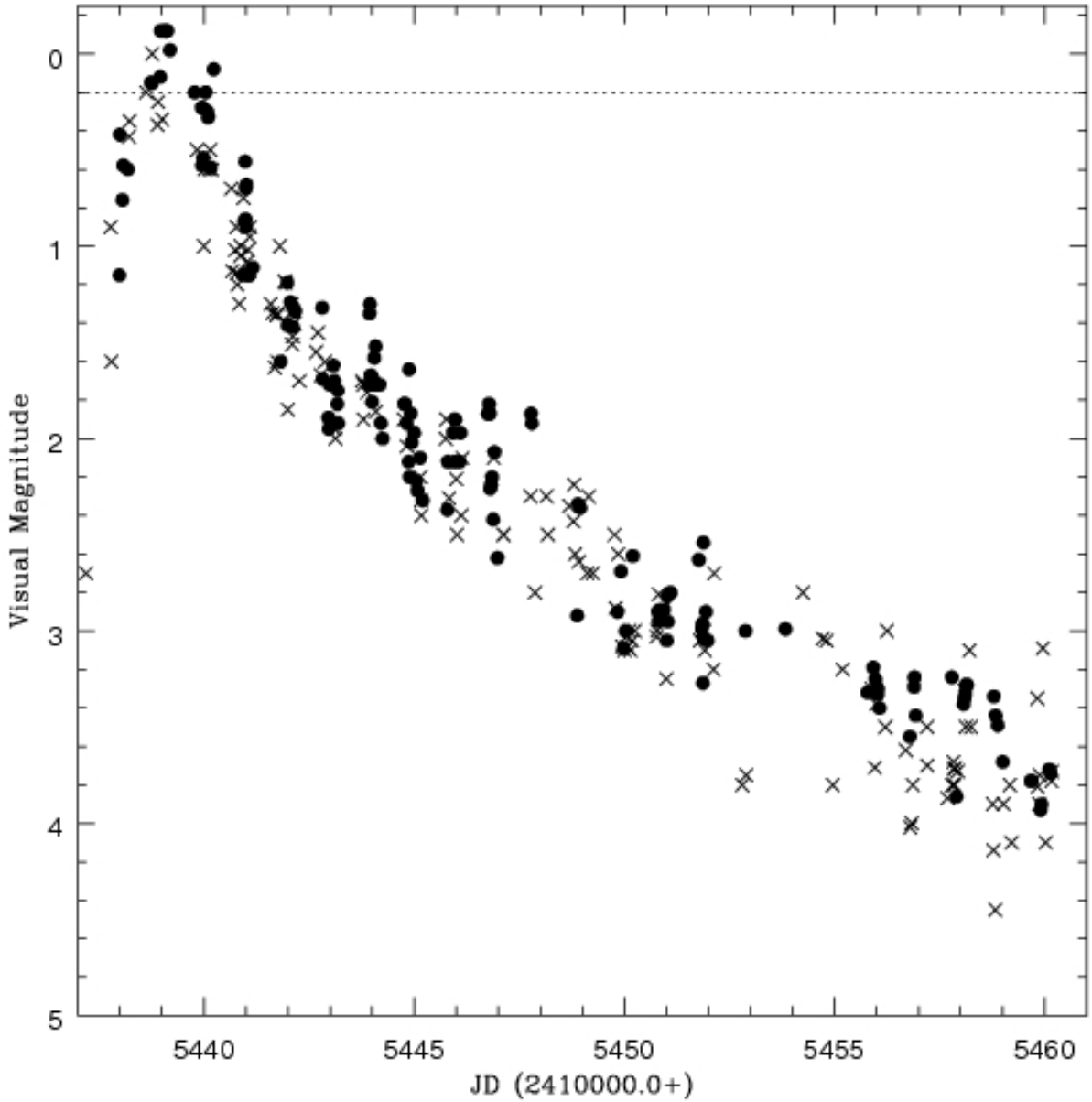


Fig. 5.— The light curve of GK Per near visual maximum using data from Campbell (1903). The solid circles are measurements where we have used modern V magnitudes for the comparison stars to recalibrate the early portion of the light curve of GK Per. The crosses are for data taken directly from Campbell. The dotted line at $m_V = 0.2$ is the commonly quoted value for its visual maximum.

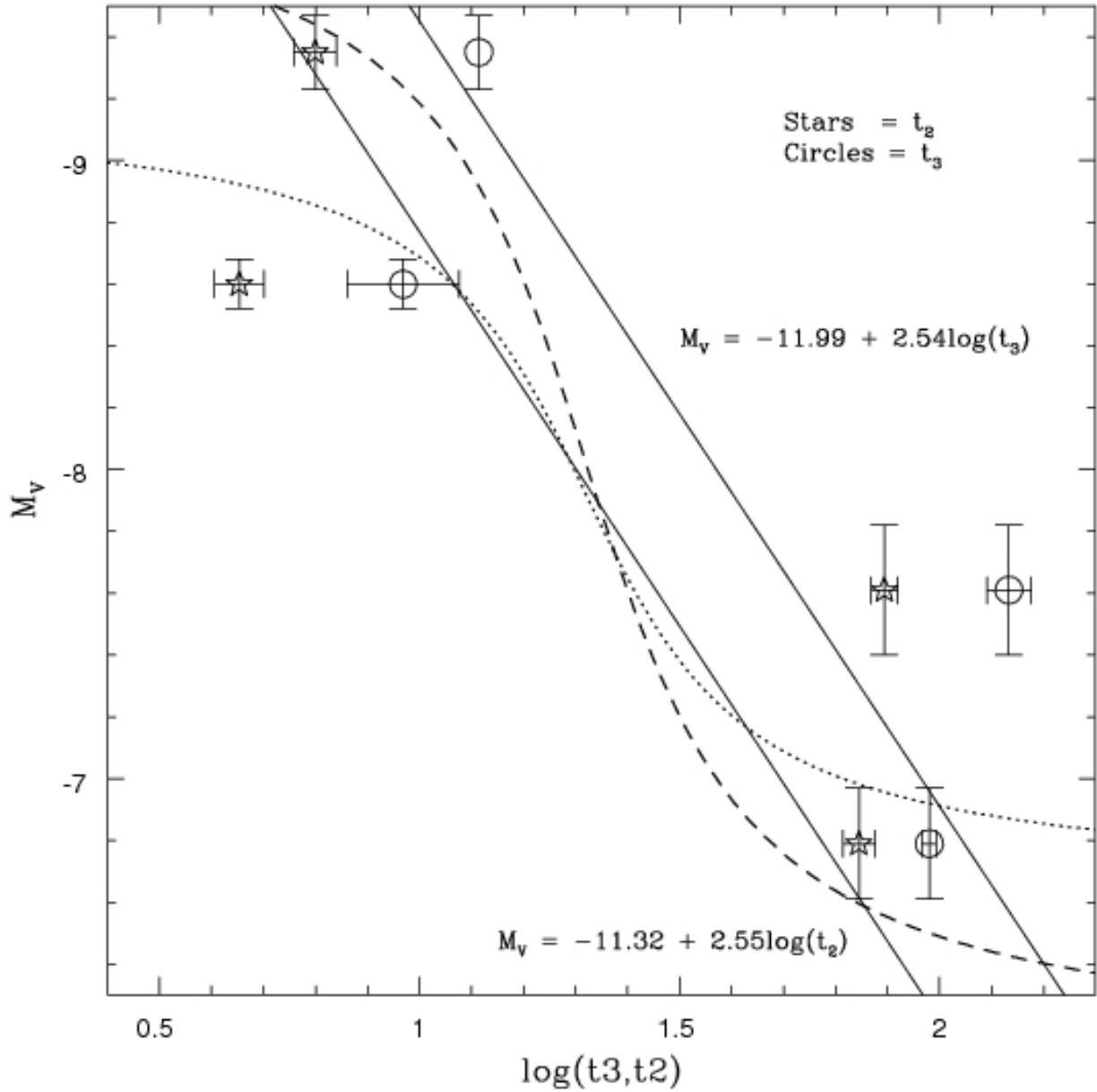


Fig. 6.— The Maximum Magnitude-Rate of Decline plot for the program novae. The linear relationships for t_2 and t_3 from Downes & Duerbeck (2000) are plotted as solid lines and labeled. The dotted line is the Della Valle & Livio (1995) arctangent relationship for t_2 , and the dashed line is this law as updated by Downes & Duerbeck. The error bars on the absolute magnitudes are those due to the error in the parallax, and do not include the uncertainty in the peak visual magnitudes of the CNe.